Fish and Shellfish Immunology 89 (2019) 647–659

Contents lists available at ScienceDirect

Fish and Shellfish Immunology

journal homepage: www.elsevier.com/locate/fsi

Full length article

Molecular cloning, characterization, and expression level analysis of a marine teleost homolog of catalase from big belly seahorse (*Hippocampus abdominalis*)

Sarithaa Sellaththurai[a], Thanthrige Thiunuwan Priyathilaka[a], Jehee Lee[a,b,*]

[a] Department of Marine Life Sciences & Fish Vaccine Research Center, Jeju National University, Jeju Self-Governing Province, 63243, Republic of Korea
[b] Marine Science Institute, Jeju National University, Jeju Self-Governing Province, 63333, Republic of Korea

ARTICLE INFO

Keywords:
Catalase
Hippocampus abdominalis
Hydrogen peroxide
Immune challenge
Cell viability

ABSTRACT

Organisms possess a cellular antioxidant defense system inclusive of ROS scavengers to maintain the homeostasis of antioxidant levels. Catalase is a major ROS scavenger enzyme that plays a significant role in the antioxidant defense mechanism of organisms by reducing toxic hydrogen peroxide molecules into a nontoxic form of oxygen and water with a high turnover rate. In the present study, we performed molecular and functional characterization of the catalase homolog from *Hippocampus abdominalis* (HaCat). The *HaCat* cDNA sequence was identified as a 1578 bp ORF (open reading frame) that encodes a polypeptide of 526 amino acids with 59.33 kDa molecular weight. Its estimated pI value is 7.7, and it does not have any signal sequences. HaCat shared a conserved domain arrangement including the catalase proximal active site signature and heme ligand signature domain with the previously identified catalase counterparts. Phylogenetic analysis displayed close evolutionary relationships between HaCat and catalases from other teleost fish. According to our qPCR results, ubiquitous expression of *HaCat* transcripts were observed in all the tested tissues with high expression in the kidney followed by liver. Significant modulations of *HaCat* transcription were observed in blood, liver, and kidney tissues post-challenge with *Streptococcus iniae*, *Edwardsiella tarda*, poly I:C, and LPS. Peroxidase activity of recombinant HaCat (rHaCat) was evaluated using an ABTS assay and the ROS removal effect was further confirmed by oxidative DNA damage protection and cell viability assays. The rHaCat showed more than 97% activity over a temperature and pH range of 10 °C–40 °C and 5 to 6, respectively. The above results suggest that HaCat plays an indispensable role in the oxidative homeostasis of the seahorse during pathogenic attack.

1. Introduction

Chemical energy is necessary for the cellular functions and survival of all organisms. Aerobic respiration is a key mechanism to achieve chemical energy in the biological system [1,2]. However, aerobic respiration under catalysis of NADPH oxidases results in the formation of reactive oxygen species (ROS). ROS include oxygen radicals, hydroxyl radicals, singlet oxygen, superoxide anion, hydrogen peroxides, and certain oxidizing agents with an ability to convert into radicals [1,3]. Superoxide (O_2^-) is one of the important ROS molecules that is formed by the reduction of one-electron from molecular oxygen. Further reduction in O_2^- by dismutation results in the formation of hydrogen peroxide (H_2O_2). Exchange of electrons between O_2^- and H_2O_2 through the Harber-Weiss reaction or reduction of H_2O_2 via Fenton reaction generates hydroxyl radicals (OH^-) [4,5]. The OH^- can damage numerous macromolecules such as lipids, proteins, carbohydrates, and nucleic acids by initiating a free radical cascade [6]. ROS as double-edged molecules play an important role in host inflammatory responses by acting directly on microorganism or inducing host inflammatory pathways as signaling molecules. However, ROS accumulation causes cell damage due to oxidation of biomolecules, DNA mutagenesis, activation of pro-cell death factors, and tumorigenesis [7,8].

In order to control ROS accumulation and maintain homeostasis, the host organisms possess a cellular antioxidant defense system inclusive of ROS scavengers. Multiple enzymes such as superoxide dismutase, catalase, glutathione peroxidase, and non-enzymatic small-molecules including reduced glutathione, vitamins E, A, and C, and ceruloplasmin are considered as potential ROS scavengers [9,10]. Superoxide dismutase activity is the first line fortification against ROS by dismutating O_2^- to H_2O_2 and H_2O [11]. The secondary defense against ROS is

* Corresponding author. Marine Molecular Genetics Lab, Department of Marine Life Sciences, College of Ocean Science, Jeju National University, 66 Jejudaehakno, Ara-Dong, Jeju, 690-756, Republic of Korea.
E-mail address: jehee@jejunu.ac.kr (J. Lee).

https://doi.org/10.1016/j.fsi.2019.03.064
Received 22 January 2019; Received in revised form 24 March 2019; Accepted 26 March 2019
Available online 29 March 2019

normally catalyzed by catalase and various peroxidases to the removal of H_2O_2 [12,13]. Among these enzymes, catalase is a major oxidoreductase enzyme that plays a crucial role by removing the toxic form of H_2O_2 by converting it to H_2O and O_2 molecules in virtually all aerobic organisms [14–16]. Two types of catalases i.e., the classical Fe heme enzymes and catalase peroxidases, are typically present in living organisms. Catalase-peroxidase also consists of a covalent triplet of distal side chains, and catalyzes peroxidatic and catalytic reactions by following different mechanisms from classical heme enzymes [17]. Monofunctional catalases are heme-containing enzymes, which are well-characterized ubiquitously expressed homo tetrameric protein with four identical subunits [18,19]. The size of the subunit is approximately 50–60 kDa [14,15]. Beta-barrel, *N*-terminal threading arm, wrapping loop, and C-terminal helixes are the four conceptual domains that exist in each subunit of human catalase [20]. Nicotinamide adenine dinucleotide phosphate-oxidase (NADPH) molecules protect the enzyme from oxidation by binding to the surface of each subunit via 12 amino acid residues [20,21]. The subcellular localization of catalase is normally in the peroxisome, where long-chain fatty acids trigger the formation of H_2O_2 by peroxisomal β-oxidation. In addition to breaking down H_2O_2 molecules produced during β-oxidation, peroxisomal catalase also acts on H_2O_2 diffusing from other sources when the intracellular H_2O_2 reaches high levels [22,23].

Along with H_2O_2 dismutation, catalase can also oxidize toxins such as phenols, formic acid, formaldehyde, and alcohols by using H_2O_2 [12,19,24]. Catalase is reported to regulate pexophagy during serum starvation by controlling ROS levels [25]. The sequence, expression, and regulation of catalase has so far been identified from many organisms including mammals [26], plants [27], and bacteria [28]. In our previous studies, catalase from black rockfish (*Sebastes schlegelii*) [29], rock bream (*Oplegnathus fasciatus*) [30] and disk abalone (*Haliotis discus discus*) [31] has been found to play an important role in oxidative stress regulation and post-innate immune responses. Studies on rock bream showed that starvation can temporarily induce catalase expression [32]. It was demonstrated that AAV-mediated delivery of catalase gene could protect retinal ganglion cells (RGCs) and the inner plexiform layer (IPL) by inhibiting the generation of H_2O_2, MDA, 8-OHdG, and nitrotyrosine during retinal ischemia/reperfusion (I/R) in rats [33]. Catalase is known to mediate an important host defense system in the gastrointestinal tract of Drosophila by regulating redox balance homeostasis during host-microbe interactions [34]. In *Marsupenaeus japonicus,* catalase was suggested to participate in intestinal host-microbe homeostasis by regulating ROS levels [35]. Catalase is considered to play a potential role in maintaining the physiological environment and innate immunity of *Chilo suppressalis* [36].

In marine bony fish species, seahorses are highly specialized species that are broadly present in temperate and tropical marine waters [37,38]. Their behaviors and traits such as low mobility, slow recolonization of overexploited areas, low population density, low fecundity, and a long period of parental care affect the fitness of the seahorse and render them vulnerable to high exploitation [38,39]. Apart from human uses, habitat loss also affects the seahorse population [40]. Seahorses are important in traditional Chinese medicine, tonics, and as aquarium decorative species [39]. However, they are listed under the “Convention on international trade in endangered species of wild fauna and flora” [41]. Commercial aquaculture of seahorses has been undertaken in several countries like New Zealand, Australia, and China [41,42]. In addition, aquaculture of big-belly seahorse with artificial reproduction was successfully achieved recently in Jeju, Korea [43]. A variety of seahorse diseases have been noted in laboratory and aquaculture observations [44]. *Vibrio harveyi* was identified as a cause of an infectious disease in the seahorse, *Hippocampus kuda* and *Hippocampus sp*. [45]. Mycobacterial infection was reported in *Hippocampus reidi* and fungal infection with *Exophiala* species was identified from *Hippocampus abdominalis* [46]. Molecular level studies on the immune defense system and an understanding of the immune response are fundamental to minimize disease and mortality. Thus identification and functional analysis of immune components from big-belly seahorse may be an effective approach for disease management and successful seahorse aquaculture maintenance. In the current study, the catalase gene from big belly seahorse *Hippocampus abdominalis* was identified and characterized. The spatial expression of *HaCat* in various tissues and its temporally modulated expression in challenge experiments was detected by qPCR. In order to confirm the activity of HaCat, protein level studies were conducted with recombinant HaCat (rHaCat). Peroxidase activity assays were performed with varying protein concentrations and biochemical conditions (Temperature and pH). Furthermore, oxidative DNA damage protection and cell protective effects during oxidative stress were evaluated using rHaCat.

2. Materials and methods

2.1. Identification and in-silico analysis of HaCat

The big-belly seahorse catalase coding sequence was identified from a previously established seahorse transcriptome database using Basic Local Alignment Tool (BLAST) in the National Center for Biotechnology Information (NCBI) server (http://blast.ncbi.nlm.nih.gov/Blast.cgi) [47]. The 454 GSFLX™ sequencing technique was used to construct the seahorse transcriptome database as described previously [48]. Different bioinformatics tools were used to characterize the identified cDNA sequence. The open reading frame (ORF) and amino acid sequence were obtained using Unipro UGENE software [49]. Conserved domains and motifs were predicted using ExPASy Prosite (https://prosite.expasy.org/) [50] and simple modular architecture research tools (SMART) (http://smart.embl-heidelberg.de/) [51]. Physical properties of HaCat were determined using the ExPASy ProtParam tool (https://web.expasy.org/protparam) [52]. Identity and similarity of HaCat protein with previously identified catalase protein sequences was predicted using the EMBOSS Needle Pairwise Sequence Alignment Tool (https://www.ebi.ac.uk/Tools/psa/emboss_needle/) [53]. Multiple sequence alignment of deduced HaCat amino acid sequence and other catalase sequences from different taxonomy was performed using the ClustalW 2.0 program [54]. The construction of phylogenetic tree was carried out in MEGA version 7.0.26 software using a neighbor-joining method with 5000 bootstrap replicates [55]. The tertiary structures of HaCat and human catalase were modeled using i-TASSER (https://zhanglab.ccmb.med.umich.edu/I-TASSER) [56,57], and the positions of active domains were visualized in the Pymol 1.7 program (https://pymol.org/2) [58].

2.2. Experimental animals

Big-belly seahorses, with an average body size of 12 cm were purchased from Korea Marine Ornamental Fish Breeding Center (Jeju Island, Republic of Korea) and maintained in laboratory aquarium tanks (300 L) with continuously aerated seawater (temperature 18 ± 2 °C and salinity 34 ± 6 psμ). Seahorses were fed twice a day with frozen Mysis shrimps and acclimatized for one week before using them in the experiments.

For tissue distribution analysis, six unchallenged seahorse individuals (average body weight of 8 g) were dissected and fourteen different tissues (blood, brain, liver, kidney, pouch, stomach, spleen, heart, gills, intestine, skin, muscle, ovary, and testis) were isolated. Blood sampling was performed by cutting the tail of experimental seahorses and blood cells were pellet out by immediate centrifugation at 4 °C for 10 min at 3000 × *g*. All collected tissue samples were immediately snap frozen using liquid nitrogen. Thereafter, the tissue samples were stored at −80 °C for further steps.

2.3. Challenge experiment

The immune responsiveness of HaCat after exposure to two live

bacteria (gram-positive *Streptococcus iniae* and gram-negative *Edwardsiella tarda*) and two immune stimulants, poly I:C (polyinosinic:polycytidylic acid, from Sigma, USA) and LPS (lipopolysaccharide, from *Escherichia coli* 055:B5; Sigma, St. Louis, MO, USA) was assessed by an *in vivo* challenge experiment. In each group, 35 acclimatized seahorses were intra-peritoneally injected separately with 100 µL of 1×10^5 CFU/µL of *S. iniae*, 1.5 µg/µL of LPS, 1.5 µg/µL of poly I:C, and 5×10^3 CFU/µL of *E. tarda* suspensions, which were prepared in sterile PBS. The control group was established by injecting 100 µL of sterile PBS. Another group of seahorses was maintained as the uninjected control. Blood, liver, and kidney samples were collected from five individuals at 3, 6, 12, 24, 48, and 72 h post injection (p.i.) as mentioned in section 2.2.

2.4. RNA extraction and cDNA synthesis

An equal amount of tissue samples collected from six healthy seahorses (for tissue distribution analysis) and five challenged seahorses at each time point (for challenge experiment analysis) were used to prepare the sample tissue pool. Total RNA was extracted from a pool of tissues using the total RNA extraction reagent RNAiso plus (TaKaRa, Japan) and was purified using the RNeasy Mini kit (Qiagen, USA). The Multiskan™ GO Microplate Spectrophotometer (Thermo Scientific, USA) was used at 260 nm to assess the concentration. The quality of extracted RNA was determined by agarose gel electrophoresis. Prime Script™ II 1st strand cDNA synthesis kit (TaKaRa, Japan) was used to synthesize the first-strand cDNA from 2.5 µg of extracted RNA. Thereafter, the synthesized cDNA samples were stored at −80 °C for further use after diluted to 40-fold.

2.5. Quantitative real-time PCR (qPCR) analysis for determination of HaCat spatial and temporal transcription pattern

Spatial and temporal *HaCat* expression was analyzed from the prepared cDNA samples (2.4) by qPCR in a Thermal cycler Dice® Real Time system III (TaKaRa, Japan). Gene specific primers for HaCat and 40S ribosomal protein S7 were designed using the PrimerQuest Tool in the IDT online server (https://sg.idtdna.com/Primerquest/Home/Index) based on their coding sequences (Table 1) [59]. The reaction mixture was prepared to a total volume of 10 µL with 3 µL of cDNA sample, 5 µL of 2 × TaKaRa Ex Taq™ SYBR premix, 0.4 µL of each forward and reverse primer (10 pmol/µL), and 1.2 µL of nuclease-free water. The PCR reaction was carried out under the following temperature profile: initial denaturation for 10 s at 95 °C; 45 PCR cycles each consisting of 5 s denaturation at 95 °C, 10 s annealing at 58 °C, 20 s extension at 72 °C; and finally 1 melting cycle with 15 s at 95 °C, 30 s at 60 °C, and 15 s at 95 °C. *Hippocampus abdominalis* 40S ribosomal protein S7 (Accession no. KP780177) was amplified under the same conditions as the internal control gene. The relative expression of *HaCat* was determined using the Livak method ($2^{-\Delta\Delta CT}$) from the average of triplicate qPCR results [60]. The *HaCat* expression changes of challenged groups were calculated with respect to the expression in the PBS injected control group.

Table 1
Primer sequences used for amplification and expression analysis of HaCat.

Name	Purpose	Sequence (5′→3′)
HaCat-F	Gene amplification	GAGAGAgatatc ATGGCTGACAGCAGAGACAAAGC
HaCat-R	Gene amplification	GAGAGAgaattc TCACATCTTGGACGAAGCGGC
HaCat -qF	qPCR	GGCAGAGGCTATGTCAGAATATGGC
HaCat -qR	qPCR	TCCGCATTGTACTTGTTGAGATGGC
40S ribosomal protein S7-qF	qPCR	GCGGGAAGCATGTGGTCTTCATT
40S ribosomal protein S7-qR	qPCR	ACTCCTGGGTCGCTTCTGCTTATT

2.6. Construction of HaCat-pMALc5X recombinant plasmid

The HaCat ORF was amplified using cDNA obtained from kidney tissue incorporating *Eco*RI and *Eco*RV restriction enzyme sites by PCR. PCR was performed with a total volume of 50 µL reaction mixture containing 5 µL of 10 × ExTaq buffer, 4 µL of 2.5 mM dNTP, 10 pmol of each forward and reverse primer, 5 µL of template DNA, 0.2 µL of ExTaq™ DNA polymerase (TaKaRa, Japan), and 33.8 µL of nuclease-free water. The TaKaRa thermal cycler was used to perform the PCR under the following physical parameters: initial denaturation for 5 min at 94 °C; followed by 30 cycles each consisting of 30 s denaturation at 94 °C, 30 s annealing at 58 °C, and 90 s extension at 72 °C; and a final extension for 7 min at 72 °C. Electrophoresis was performed on 1% agarose gel to separate the PCR products. The amplified gene band was excised from agarose gel and purified using the AccuPrep™ Gel Purification Kit (Bioneer, Korea). The pMAL-c5X vector (New England BioLabs, USA) and purified gene products were digested using *Eco*RI and *Eco*RV restriction enzymes (TaKaRa, Japan). The digested pMAL-c5X and gene product were ligated using Mighty Mix (TaKaRa, Japan) at 16 °C for 30 min using TaKaRa thermal cycler followed by overnight incubation at 4 °C. The resulting recombinant plasmid was sequenced after transformation into *E. coli* DH5α competent cells.

2.7. Overexpression and purification of HaCat protein

Sequence confirmed recombinant plasmid was transformed into *E. coli* BL21 (DE3) competent cells for protein expression. Transformed *E. coli* BL21 (DE3) were grown in 500 mL LB medium supplemented with glucose (final concentration of 2.0 gL^{-1}) and ampicillin (final concentration of 100 µg/mL) at 37 °C/200 rpm. The culture was induced with isopropyl-β-D-1-thiogalactopyranoside (IPTG, 0.5 mM) when the OD_{600} reached a value of 0.6 and was further incubated at 20 °C/200 rpm for 8 h. Thereafter the culture was cooled by keeping on ice for 20 min, and cells were harvested by centrifugation (1200 × *g* for 20 min). The pellet was resuspended in column buffer (20 mM Tris-HCl, 200 mM NaCl, and 1 mM DTT at pH 7.4), recentrifuged at 1200 × *g* for 20 min, and frozen at −20 °C. The cells were thawed in running cold water and resuspended in 40 mL of column buffer. Resuspended cells were lysed using cold sonication and then centrifuged for 20 min at 9000 × *g*. The supernatant was mixed with 1 mL of amylose resin (New England Biolabs, USA) and mixed for 10 min in order to achieve better binding. The resin and supernatant mix was loaded on the column and washed with 12 mL of column buffer. Finally the recombinant protein (rHaCat) was collected as fractions using the elution buffer (Column buffer containg 20 mM maltose). Protein concentration was estimated using the Bradford method [61]. The purity of the purified protein was confirmed by SDS-PAGE (sodium dodecyl sulfate polyacrylamide gel electrophoresis).

2.8. Hydrogen peroxide scavenging activity of rHaCat

Peroxidase activity of rHaCat was estimated by ABTS assay using varying protein concentrations. The method was used as described in a previous report with some modifications [62]. The rHaCat was dissolved in 1% PBS to a final volume of 120 µL (with varying protein amounts) and loaded in a 96-well plate. The plate was kept in 25 °C incubator for 5 min after adding 20 µL of 10 mM H_2O_2. The remaining H_2O_2 was determined by a second incubation at 37 °C with 30 µL of 2,2'-azino-bis(3-ethylbenzothioline-6-sulphonic acid) (ABTS) and 30 µL of 1 U/ml peroxidase. The developed blue-green color by the formation of ABTS cations was then measured at 405 nm using a multi-plate reader (Thermo Scientific, Waltham, MA, USA). In addition, the same assay was repeated with recombinant maltose binding protein (rMBP) and a

control experiment was carried out without the protein. All reactions were carried out in triplicate, and the average absorbance results were used for the calculations.

2.9. Biochemical properties of rHaCat

In order to characterize the effect of temperature and pH on the enzymatic activity of rHaCat, the antioxidant assay was performed with a temperature and pH gradient. An amount of 50 μg rHaCat was used in each reaction. In the effective temperature assay, eight different temperatures were selected with 10 °C increments starting from 10 °C. During the assay, hydrogen peroxide was added to the reaction mixture at the selected temperatures and was incubated for 5 min; all other steps were followed as mentioned in section 2.8. The pH gradient was maintained at 1.0 pH intervals from pH 4.0 to pH 10.0 using sodium bicarbonate, sodium carbonate, sodium phosphate monobasic, sodium phosphate dibasic, and citric acid, and the experimental procedure was followed as described in section 2.8. Control assays were performed with rMBP or without any proteins. All the reactions were carried out in triplicate.

2.10. Evaluation of rHaCat protective effect against oxidative DNA damage

In order to evaluate the shielding of DNA by rHaCat from oxidative damage, an MFO assay (Thiol mixed-function oxidation assay) was carried out with different concentrations of rHaCat, rMBP, and without any protein as a control [63]. Reaction mixtures were prepared in a total volume of 20 μL, with a final concentration of 40 μM of Fe(III) chloride, 10 mM of DTT (dithiothreitol), and 25 mM of HEPES (hydroxyethyl-piperazineethane-sulfonic acid buffer). The mixtures were incubated at 25 °C for 10 min after enzyme addition. Thereafter the pUC19 plasmid DNA (1 μg) was added to the mixture and kept in 37 °C incubator for 10 min. Soon after incubation, DNA was purified from each reaction mixture using the AccuPrep® PCR purification kit (Bioneer, Korea), according to the manufacturer's procedure. Conformations of DNA after the reaction was interpreted by agarose gel electrophoresis.

2.11. Cell protective effects of rHaCat during oxidative stress

To investigate the effect of rHaCat on cell viability during oxidative stress, MTT assay was performed using the Vero cell line derived from African green monkey kidney. The experiment was performed following a previous report with some modifications [64]. Cells were cultured in a 5% CO_2 humified incubator at 37 °C in RPMI 1640 culture medium containing 10% FBS with penicillin (100 U/mL) and streptomycin (100 U/mL). Vero cells (2×10^5 cells/mL) were seeded in a 96-well plate and cultured for 24 h. The cells were pretreated with proteins (rHaCat and rMBP) for 30 min prior to H_2O_2 treatment. The experimental and control cells were maintained as follows: (1) Untreated control cells; (2) Cells treated only with H_2O_2; (3) Cells pretreated with rMBP (100 μg/mL) prior to H_2O_2 treatment; (4) Cells pretreated with rHaCat (25 μg/mL) prior to H_2O_2 treatment; (5) Cells pretreated with rHaCat (50 μg/mL) prior to H_2O_2 treatment; (6) Cells pretreated with rHaCat (75 μg/mL) prior to H_2O_2 treatment; (7) Cells pretreated with rHaCat (100 μg/mL) prior to H_2O_2 treatment. Cells were then treated with H_2O_2 (final concentration of 500 μM) and incubated for 24 h. MTT assay was used to detect cell viability [65]. Yellow tetrazolium MTT (3-(4,5-dimethyl thiazolyl-2)-2,5-diphenyl tetrazolium bromide) solution (2 mg/mL) was added to each well at 50 μL and incubated for 3 h. Finally, the medium with MTT solution was aspirated, 150 μL of DMSO (dimethylsulfoxide) was added to dissolve the purple formazan, and absorbance at 540 nm was measured using an ELISA plate reader (Synergy HT, Biotec, Korea). Viability of control cells (1) was considered as 100% to calculate the percentage cell-viability of treated cell samples and the results were expressed as the mean of triplicate assays.

2.12. Statistical analysis

All qPCR, ABTS, and MTT assays were performed in triplicate and the data are shown in graphs as the mean ± standard deviation (SD). To determine statistical significance ($p < 0.05$) between experimental and control groups, Student's *t*-test was applied to the data.

3. Results

3.1. Identification and sequence characterization of HaCat

HaCat contains 526 amino acids encoded by a 1578-bp ORF with the following physical properties; a theoretical isoelectric point of 7.7 (58 negatively charged residues and 59 positively charged residues) and a molecular mass of 59.53 kDa. A signal peptide was not found. The HaCat sequence data were submitted to NCBI-GenBank sequence database under the accession number MK404533. *In silico* analysis of the protein sequence showed that HaCat consists of a catalase proximal active site signature domain (residues 64–80) and proximal heme ligand binding signature (residues 354–362). HaCat also exhibits highly conserved amino acid sequences including “FDRERIPERVVHAKGAG” (proximal active site signature) and “RLFSYPDTH” (proximal heme ligand signature) with diverse species (Fig. 1). Furthermore, conserved structures in the heme ligand binding pocket, NADPH binding sites, and tetramer interface with human erythrocyte catalase were also identified.

Pairwise sequence alignment analysis of HaCat resulted in 94.5% similarity and 88.2% identity with Rock bream catalase. Catalase amino acid sequences from *Seriola lalandi dorsalis, Homo sapiens, Columba livia,* and *Drosophila melanogaster* also exhibited sequence specific identities of 87.7%, 76.9%, 76.2%, and 62.4% with HaCat, respectively (Table 2). The phylogenetic analysis outcome of HaCat with catalase amino acid sequences from 17 typical species shows two main clusters, as vertebrates and invertebrates, using bacterial catalase (*Rhizoctonia solani)* as the outgroup. As expected, HaCat was sub-clustered with fish sequences (Fig. 2).

3.2. Prediction of tertiary structure for HaCat

Correlation between the functional and structural properties of HaCat was predicted using 3D structure, which was hypothetically modeled using the i-TASSER online server. Similarity between both human and seahorse catalase structures was observed clearly through the domain arrangement. Moreover, the basic amino acid residues Asp 141, His 75, His 364, His 362, Tyr 358, Arg 354, and Tyr 370, which are essential to maintain the electronic circuit for complete enzyme activity were visualized in both HaCat and human catalase (Fig. 3).

3.3. Tissue distribution of HaCat

HaCat expression was ubiquitously observed in all tested tissues by a qPCR assay. The expression fold of *HaCat* in each tissue was calculated relative to the testis. The prominent expression of *HaCat* was observed in the kidney followed by the liver and stomach (Fig. 4).

3.4. Temporal expression of HaCat

To examine the post-immune responses of HaCat, transcripts levels of *HaCat* at different time points after challenge experiments were determined by qPCR. The expression profile of *HaCat* in liver tissue is depicted in Fig. 5A. LPS stimulation resulted in significant upregulation at 48 h and significant downregulations at 3 h, 6 h, 12 h, 24 h, and 72 h. Early stage significant upregulation at 3 h and significant downregulation at 6 h to 48 h was observed with poly I:C stimulation. Immune stimulation with both live bacteria, *E. tarda* and *S. iniae* resulted in significant downregulation from 3 h to 72 h.

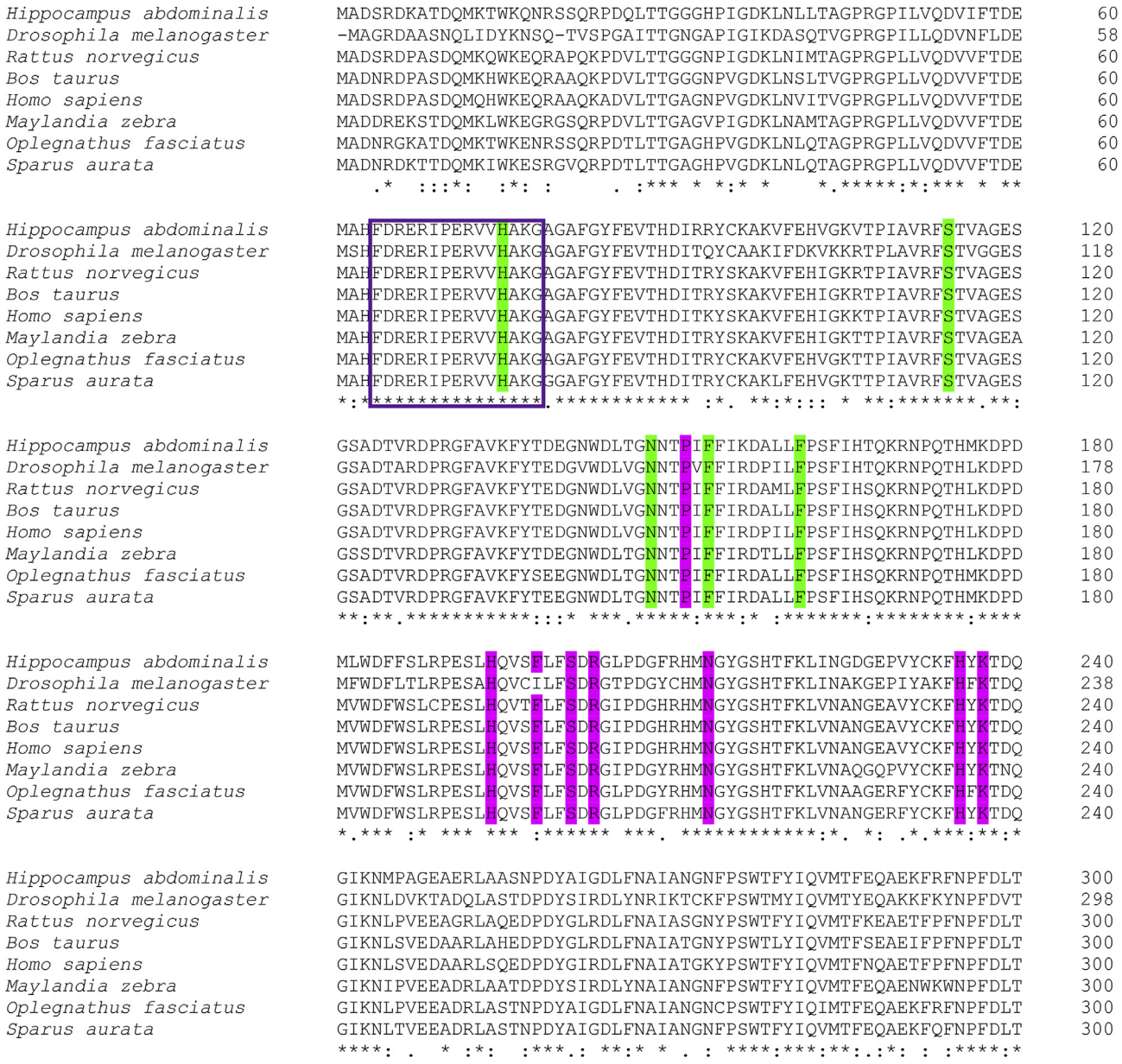

Fig. 1. Results obtained from Clustal W multiple sequence alignment of HaCat with some other vertebrate catalases. The catalase proximal active site signature domain (64–80) and proximal heme ligand binding signature (354–362) are boxed in purple and red, respectively. Purple and green shading indicate the NADPH-binding sites and heme-binding sites. (For interpretation of the references to color in this figure legend, the reader is referred to the Web version of this article.)

The *HaCat* transcript level in blood with time post challenge is shown in Fig. 5B. After LPS admistration, *HaCat* was significantly elevated at 3 h p. i., whereas significantly downregulated transcript levels were detected at 12 h and 48 h p. i. Significant upregulation was observed at 3 h and 72 h in the poly I:C stimulated group. The *E. tarda* stimulated group showed significant upregulation at 3 h, 24 h, and 72 h. Similar to the LPS challenge, upregulated *HaCat* mRNA expression was detected only at 3 h p. i. with *S. iniae*. Thereafter, the transcript level remained unchanged or in a downregulated state throughout the experiment.

Following stimulation with LPS, the transcript level of *HaCat* in kidney (Fig. 5C) was significantly upregulated at 3 h and 6 h p. i., while significant downregulation was observed at 12 h, 24 h, and 48 h p. i. Post challenge with polyI:C, significant downregulation of transcript levels was observed at 3 h, 6 h, 12 h, 24 h and 48 h p. i. Early phase significant upregulation at 3 h and 6 h p. i., followed by continuous and significant downregulation at 12 h, 24 h, 48 h and 72 h p. i. was observed after stimulation with *E. tarda*. Immune stimulation with *S. iniae* resulted in continuous and significant downregulation at 3 h, 12 h, 24 h, 48 h and 72 h p. i.

3.5. Overexpression and purification of rHaCat

The rHaCat was overexpressed using the *E. coli* BL21 (DE3) cells. The target protein was purified using amylose resin, and samples collected during the protein purification steps (total cell extract, supernatant, and final purified protein) were analyzed by SDS–PAGE. Two bands were observed on the gel for rHaCat, of which one band was obtained with a size of 102 kDa (59.5 kDa of HaCat + 42.5 kDa of MBP) as expected (Fig. 6).

3.6. Hydrogen peroxide scavenging activity

Hydrogen peroxide scavenging activity of rHaCat was measured

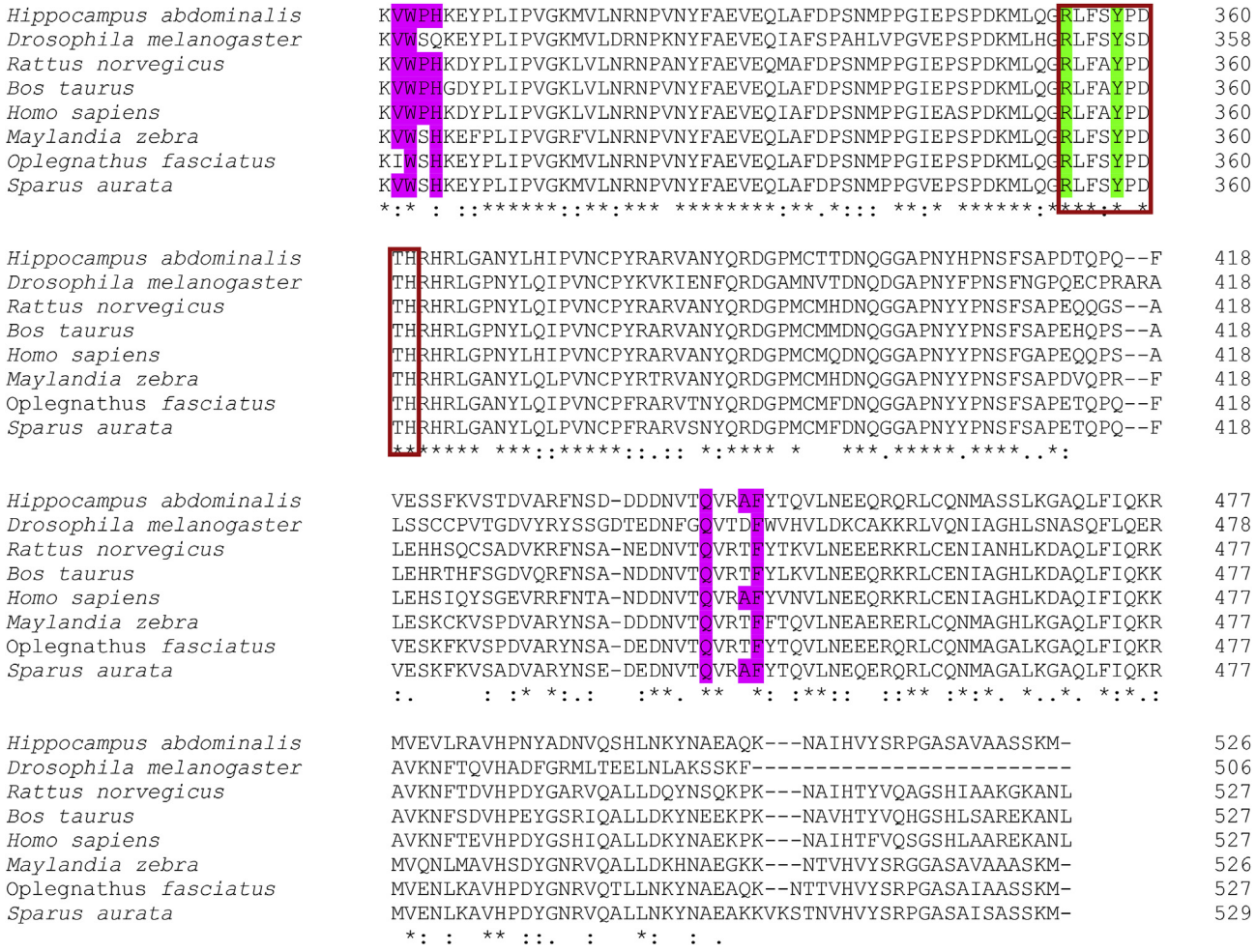

Fig. 1. (*continued*)

against different protein concentrations and plotted with the activity of rMBP (Fig. 7). The percentage of scavenging activity was increased with increasing protein concentration, high activity was obtained at a final rHaCat concentration of 250 μg/μL, and it remained constant with high protein concentrations. No significant activity of rMBP was observed (Fig. 7).

3.7. Effects of biochemical properties on rHaCat activity

The influence of pH and temperature on the hydrogen peroxide

Table 2
Percentage sequence similarity and identity of the HaCat amino acid sequence with various catalase homologs.

Species Name	Taxonomy	NCBI Accession No	Amino Acids	Identity%	Similarity%
Oplegnathus fasciatus	Fish	AAU44617.1	527	88.2	94.5
Seriola lalandi dorsalis	Fish	XP 023256083.1	527	87.7	93.5
Totoaba macdonaldi	Fish	ARM65440.1	527	87.5	94.9
Oryzias sinensis	Fish	AKG51681.1	527	86.1	94.3
Rachycentron canadum	Fish	ACO07305.1	527	87.1	94.1
Amphiprion ocellaris	Fish	XP 023141577.1	527	86.7	94.1
Sparus aurata	Fish	AFV39797.1	529	86.6	94.0
Maylandia zebra	Fish	XP 023009849.1	527	87.1	93.9
Rattus norvegicus	Mammalia	AAB42378.1	527	77.7	88.3
Canis lupus familiaris	Mammalia	BAB20764.1	527	77.1	87.5
Homo sapiens	Mammalia	NP 001743	527	76.9	87.3
Felis catus	Mammalia	XP 003993206.1	527	77.3	87.1
Columba livia	Aves	PKK29303.1	528	76.2	87.1
Bos taurus	Mammalia	NP001030463.1	527	77.8	86.7
Amazona aestiva	Aves	KQK76540.1	528	74.6	86.7
Xenopus laevis	Amphibia	ABK62836.1	528	75.8	85.8
Fenneropenaeus chinensis	Crustaceans	ABW82155.1	520	66.4	77.0
Exaiptasia pallida	Anthozoa	KXJ18065.1	509	63.5	75.5
Haliotis discus discus	Mollusca	ABQ60044.1	501	60.5	75.5
Drosophila melanogaster	Insecta	NP 536731.1	506	62.4	74.7
Rhizoctonia solani	Bacteria	CCO32660.1	411	28.1	39.4

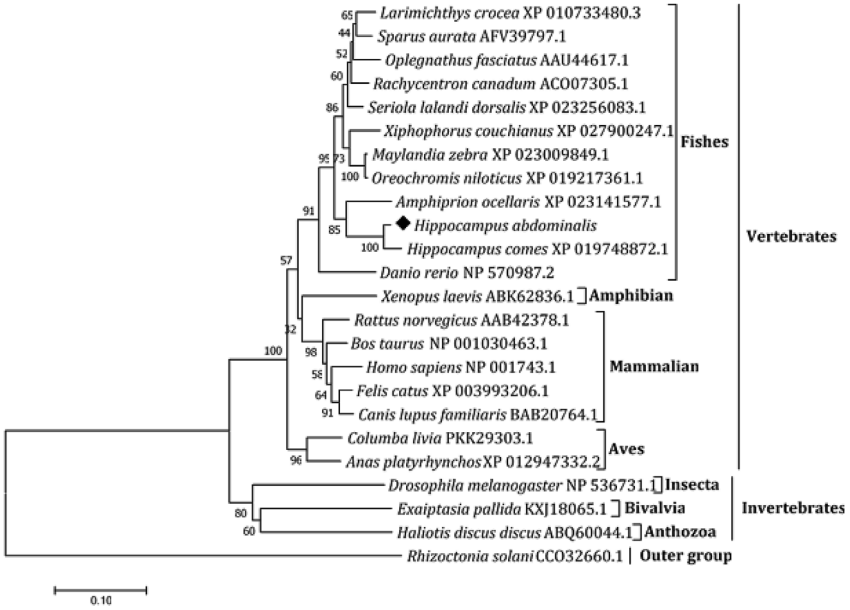

Fig. 2. Phylogenetic tree of various catalase protein sequences including HaCat generated with MEGA version 7.0.26 software using the neighbor-joining method. Bootstrap values are mentioned on the branches.

scavenging activity of rHaCat was investigated with a range of pH and temperatures. Analyzed results were plotted for temperature and pH gradients in Fig. 8A and Fig. 8B respectively. Activity of rHaCat was high at 10 °C within our temperature gradient range. Residual activity was maintained at higher than 97% until 40 °C and was then reduced to 63% within 40 °C–50 °C, and was further reduced to 10% in the range of 50 °C–60 °C. Significant activity changes were not observed for rMBP (Fig. 8B). Optimum rHaCat activity was obtained at pH 6. Moreover, the activity was maintained at more than 97% in pH range of 5–6 and then dramatically reduced with increment in the pH. The activity of rMBP was maintained at less than 11% at all tested pH values (Fig. 8A).

3.8. Protection of DNA from oxidative damage by rHaCat

Purified DNA samples were run on 1% agarose gel with untreated pUC19 plasmid to compare the plasmid conformation. No supercoiled conformations were detected in the reaction with rMBP and a negative control without any proteins (Fig. 9). However, samples from reaction mixtures with rHaCat showed intense bands belonging to supercoiled pUC19, with increasing concentration of rHaCat protein. Further, the intensity of the nicked form of pUC19 was reduced with increasing amounts of rHaCat (Fig. 9).

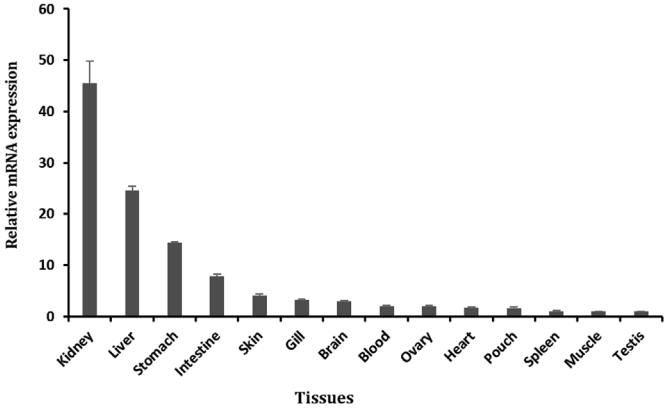

Fig. 4. Tissue-specific transcription of *HaCat* in unchallenged seahorses measured by qPCR analysis and the results calculated using the Livak method. The seahorse 40S ribosomal protein S7 was used as an internal control gene. Fold-change in *HaCat* expression is shown relative to the mRNA expression level in testis tissue. Standard deviations (SD) of the triplicates (n = 3) are presented by the error bars.

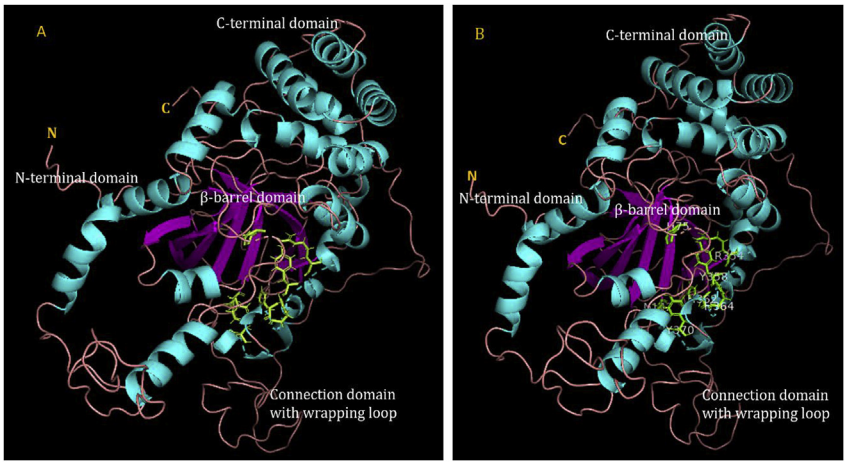

Fig. 3. The 3D model comparison of seahorse (A) and human (B) catalases. Purple-colored β-sheets and dull blue colored α-helixes are connected through brown colored loop forms. The green color stick structure indicates the amino acids (Asp 142, His 75, His 364, His 362, Tyr 358, Arg 354, and Tyr 370) that are essential for complete enzyme activity. (For interpretation of the references to color in this figure legend, the reader is referred to the Web version of this article.)

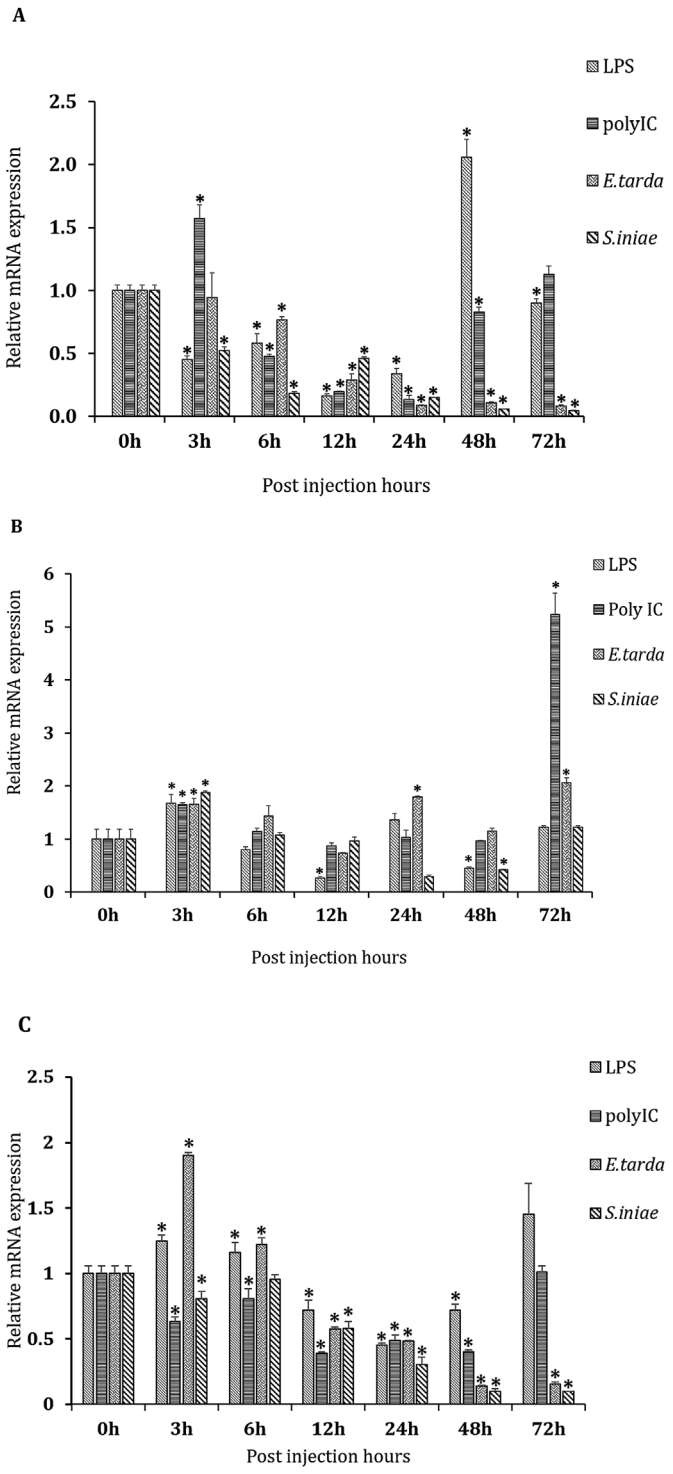

Fig. 5. Temporal mRNA expression level of *HaCat* in seahorse liver (A), blood (B) and kidney (C) tissues following LPS, poly I:C, *E. tarda,* and *S. iniae* stimulation. The relative *HaCat* transcript levels were determined using the Livak method. Seahorse 40S ribosomal protein S7 was used as the internal control gene. Expression levels of HaCat at each time point were further normalized to those of the PBS injected control. The asterisk marks (*) in the graph represent the significance ($P < 0.05$) of the transcription level calculated by Student's *t*-test corresponding to the transcription level of the 0 h control.

3.9. Cell protective effect of rHaCat during oxidative stress

Cell protective effects of HaCat under oxidative stress were determined using the MTT assay with the purified rHaCat fusion protein.

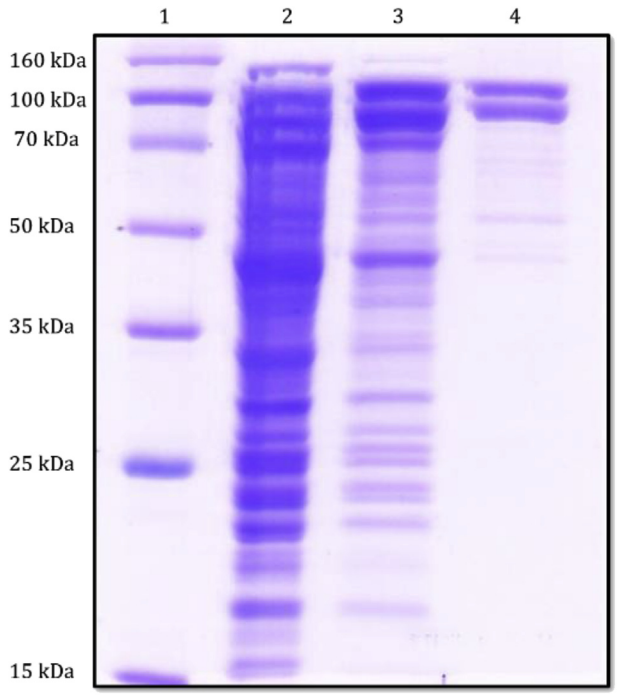

Fig. 6. SDS-PAGE analysis of purified rHaCat protein. Lane 1, protein ladder; Lane 2, Total extract of uninduced *E. coli* BL21 cells containing the HaCat-pMAL-c5X expression vector; Lane 3, Supernatant after sonication; Lane 4, purified rHaCat protein.

The analyzed results were represented in a graph as percentage cell-viability of Vero cells (control, rMBP treated, and rHaCat treated) under the oxidative stress induced by H_2O_2 (Fig. 10). Percentage cell-viability was increased with increasing concentration of rHaCat. A significant increase in cell viability was observed only with rHaCat treated samples and not with rMBP treated samples.

4. Discussion

Maintaining the homeostasis of cellular proteins is imperative in organisms to execute all the necessary functions for their survival. Imbalance in protein homeostasis may cause disease conditions or cellular malfunction. Oxidative stress can damage all cellular macromolecules including proteins [66]. Maintaining the cellular antioxidant levels is a substantial role of the antioxidant defense pathway, and is achieved by a group of antioxidant enzymes including catalase. In this study, we characterized the catalase gene from *Hippocampus abdominalis*. The characterized HaCat was found to be in the size range of 460–590 amino acids with an approximate molecular mass of 50–60 kDa, which is usually observed in prokaryotes and eukaryotes [14,15]. By multiple sequence alignment, the catalase proximal active site signature domain and proximal heme ligand binding signature of HaCat was found to be highly conserved with that of other vertebrate catalases. Recent studies have illustrated that a charge-relay network may be needed for catalytic and peroxidase activity of catalases to maintain the reaction intermediates in a steady state and to promote peroxide cleavage. The above mechanism has been speculated to control the activity of catalase by diminishing the cationic charge of the porphyrin-radical and forming an electron deficient oxyferryl moiety at Tyr 358 [19]. The above mentioned Tyr 358 is present in the HaCat sequence. This charge relay network originates from the positions of amino acid residues further upheld by linking between catalase monomers. This electronic network facilitates high substrate turnover and drives the overall reaction through a coupled enzymatic reduction in one heme molecule with corresponding oxidation at the linked heme

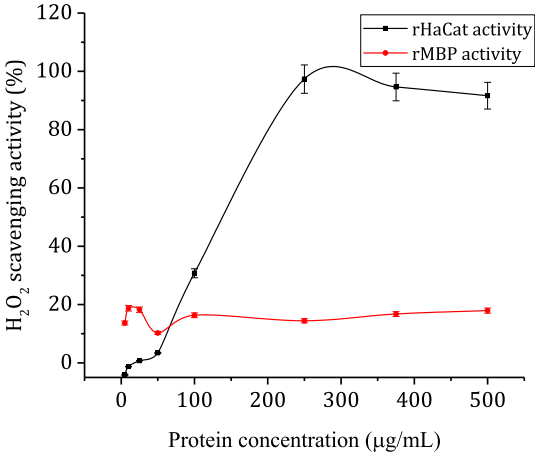

Fig. 7. Effect of rHaCat fusion protein and rMBP protein concentration on hydrogen peroxide scavenging activity.

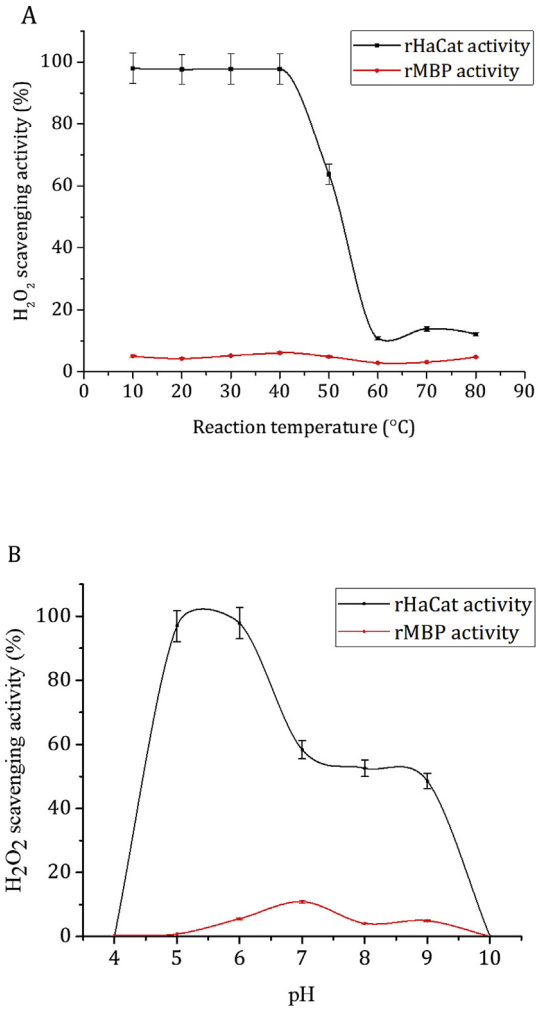

Fig. 8. Alterations in the percentage peroxidase activity of rHaCat and rMBP under a temperature (A) and pH gradient (B).

molecule. Amino acid residues of Asp 141, His 75, His 364, His 362, Tyr 358, Arg 354, and Tyr 370 have been found as basic residues for full enzyme activity, which are essential in the above electronic circuit [18]. Among these, all residues are present in the HaCat sequence except for Asp 141. However, the HaCat sequence contains Asp 142, and this position variation is also found in some other vertebrates including

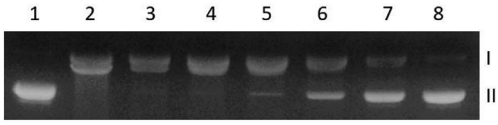

Fig. 9. Oxidative damage protection of plasmid DNA by rHaCat, analyzed by MFO assay. Gel electrophoresis results after DNA purification. Lane 1, Untreated pUC19 plasmid DNA; Lane 2, plasmid DNA from the reaction mixture without any protein; lane 3, plasmid DNA from rMBP treated reaction mixture; Lanes 4–8, purified plasmid DNA from HaCat treated reaction mixture (Final concentration of HaCat used in the reaction mixture: Lane 4–0.05 μg/μL, Lane 5–0.1 μg/μL, Lane 6–0.25 μg/μL, Lane 7–0.5 μg/μL, and Lane 8–0.75 μg/μL). Band I and II indicate the nicked form and supercoiled form of pUC19 plasmid, respectively.

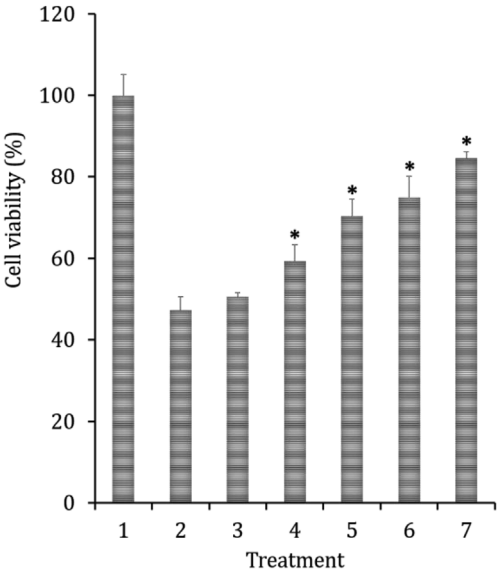

Fig. 10. The effect of rHaCat on Vero cell viability upon exposure to 500 μM H_2O_2. Treatments: (1) control cells; (2) cells treated with H_2O_2; (3) cells treated with rMBP (100 μg/mL) prior to H_2O_2 treatment; (4) cells treated with rHaCat (25 μg/mL) prior to H_2O_2 treatment; (5) cells treated with rHaCat (50 μg/mL) prior to H_2O_2 treatment; (6) cells treated with rHaCat (75 μg/mL) prior to H_2O_2 treatment; (7) cells treated with rHaCat (100 μg/mL) prior to H_2O_2 treatment. MTT assay was carried out in triplicate for each treatment. The asterisk (*) represents significant differences in the percentage cell viability of protein (rHaCat and rMBP) pretreated Vero cells against the untreated samples (Treatment 2) ($P < 0.05$).

the human catalase sequence (Fig. 1). In addition, HaCat exists as a tetramer arrangement framed by four identical subunits. Tetramerization is suggested as crucial for the function of various catalases including human catalase [20]. The striking similarities in domain arrangement and the position of active amino acids present in the 3D structure of human catalase and HaCat, which was modeled using the I-TASSER online server, suggest their functional analogy (Fig. 3). The above sequence arrangement clearly exhibits the functional and structural relationship of HaCat with previously identified catalases. The evolutionary relationship of HaCat with known catalase counterparts was evaluated by phylogenetic analysis. The clustering pattern of the phylogenetic tree confirms the common vertebrate ancestral origin of HaCat. Moreover, HaCat was highly related to the catalase of *Amphiprion ocellaris*.

According to the results of tissue distribution analysis, HaCat was ubiquitously expressed in all examined tissues and a high level of expression was observed in the kidney followed by the liver and stomach. In teleost fishes, blood pathogens are notably trapped in the kidney and spleen [67]. Seahorses have an aglomerular kidney that consists of well-developed hemopoietic foci with free macrophages [68,69].

Macrophages are involved in the defense mechanisms by phagocytosis of pathogenic microorganisms [70]. By increasing catalase production, macrophages evade H_2O_2-induced apoptosis in high oxidative environment [71]. This may be a reason for the observed highest expression of HaCat in kidney. Typically, high levels of antioxidant enzymes could be observed in the liver due to the high oxidative stress generated by excessive ROS production during the process of detoxification and xenobiotic metabolism [72–74]. It has been recorded that, the mRNA of Cu/Zn-SOD, Mn-SOD, GPx1a, GR, GPx 1b, and catalase is highly expressed in the liver of river pufferfish [72]. In freshwater teleosts, the kidney and liver tissues were observed to have a significant role in antioxidant defenses during cadmium-induced oxidative stress [75]. The highest basal expression of catalase was detected in liver tissues of *Onychostoma macrolepis* [76]. Moreover, studies focused on black rockfish and rock bream demonstrated the highest mRNA expression of catalase in liver tissues followed by the blood in unchallenged animals [29,30]. Moreover, variations of HaCat mRNA levels in different tissues of seahorse reflect the differential level of catalase activity with respect to the oxidative levels of those tissues.

In order to understand the role of HaCat in immune responses during pathogenic infection, the temporal changes in *HaCat* transcription were examined by qPCR with cDNA prepared from two highly expressed tissues (liver, kidney) and blood at different time points post-immune challenge. The liver plays a central role in the regulation of inflammation by generating anti-inflammatory proteins and cytokines. Moreover, the liver receives blood directly from the gut, which further exposes the liver to foreign materials [77]. Further, catalase plays an essential role in maintaining the oxidative level in blood to protect hemoglobin from oxidative breakdown [78]. *HaCat* expression was significantly upregulated at 3 h post challenge in the liver only upon poly I:C stimulation and in kidney following stimulation with LPS and *E. tarda*. However, significantly elevated *HaCat* mRNA was detected at 3 h p. i. of all four stimulants in blood. This observation can be an effect of low basal expression in blood compared to that in kidney and liver. Basal expression of *HaCat* in blood may not be adequate level to tolerate the oxidative stress produced by the host defense system in response to live bacteria or PAMPs. The transcript levels were significantly downregulated during mid-phase time points in liver (6 h, 12 h, and 24 h p. i.) and kidney (12 h, 24 h, and 48 h p. i.) with all four stimulants; the transcript levels were downregulated in the blood at 12 h and 24 h p. i. with LPS and *S. iniae,* respectively. Previously, significant downregulation of catalase mRNA was observed at 6 h after administration of poly I:C in rock bream blood [30]. This mid-phase down-regulation may be a result of mRNA turnover in order to increase the ROS levels in host cells [79]. ROS can kill pathogenic microorganisms via direct contact at the early stages of infection or through an indirect manner by stimulation of pathogen elimination using non-oxidative mechanisms like pattern recognition receptors signaling, neutrophil extracellular trap formation, autophagy, and lymphocyte responses [80,81]. At this stage, catalase expression should be limited to prevent the degradation of H_2O_2; however, high levels of H_2O_2 are also toxic to seahorse cells. The observed upregulation of *HaCat* transcripts in later phases might be to overcome the adverse effects produced by H_2O_2. However, the transcript level of *HaCat* in liver and kidney following stimulation with both live bacteria resulted in continuous downregulation throughout the experimental period, except for the upregulation of *HaCat* observed in kidney at 3 h and 6 h p. i. with *E. tarda* stimulation. The anatomy and populations of cells (Kupffer cells, nuclear killer cells, natural killer T, and reticuloendothelial cell) in the liver enable this organ to detect and respond to infectious organisms [82]. Liver macrophages (Kupffer cells) were identified to play a role in rapid bacterial capture and elimination [83]. A sequential light microscopic and ultrastructural study on the uptake and handling of *Vibrio salmonicida* in phagocytes of the head kidney in Atlantic salmon demonstrated the active and rapid removal of live bacteria and scavenging of cellular degradation products by the action of phagocytes and melanomacrophages [84]. Moreover, elevated ROS levels can activate some transcription factors like NF-κB to boost the inflammatory cascade [85]. According to the above mentioned references, rapid removal of infectious organisms, and the need for ROS to activate inflammatory pathways might be the reasons for the observed downregulation of catalase in kidney and liver following bacterial stimulation. The same pattern of expression was observed in black rockfish with *S. iniae* [29]. Based on the observed fluctuations in *HaCat* transcription after the challenge experiment, we suggested that the HaCat has a potential role in seahorse immunity during pathogenic infection.

SDS-PAGE analysis confirmed the overexpression of HaCat by IPTG induction and purification with amylose resin. Catalase can undergo epigenetic modification mainly by proteolysis and form truncated forms of the original enzyme [86,87]. This might be the reason that we obtained two bands in SDS-PAGE for HaCat. Similar double band patterns have been observed previously with black rockfish [29], rock bream [30], and disk abalone [31] catalases.

rHaCat activity was determined by examining the hydrogen peroxide scavenging activity with different concentrations of rHaCat. Increased activity with concentration was observed until the concentration was optimum for the reaction (250 μg/mL). The plotted graph shows the log phase within 50–250 μg/mL of the final protein concentration (Fig. 7). During this limit, the obtained straight line indicates the zero order reaction [88]. After the optimum concentration, the activity was in the steady state, even though the concentration of the protein was increased. The rMBP did not show any activity with varying concentration. The optimum protein concentration was used to analyze the biochemical properties of the rHaCat protein. During our former studies, recombinant catalases were found to possess relative enzymatic activity with a wide-range of temperatures. Percentage activity of rock bream catalase was observed to be constant from 10 °C to 80 °C [30] and the relative activity of abalone catalase was recorded without significant fluctuation until 70 °C [31]. However, in the present study, rHaCat activity began to decrease after 40 °C. A broad range of heat stability was observed in previous studies for various catalases purified from different organisms. An optimum temperature of 90 °C was recorded for *Pyrobaculum calidifontis* strain VA1 catalase [89]. Therefore, the effect of temperature might depend on the type of species. Some other immune related enzymes from big-belly seahorse were also reported to with temperature stability similar to rHaCat, such as glutathione S-transferase [90] and G-type lysozyme [91]. Usually most animal enzymes are rapidly denatured at temperatures above 40 °C [88]. The above observations suggest that rHaCat can suffer H_2O_2 mediated oxidative stress over a wide range of temperatures from very low temperature (10 °C). Activity decay of enzymes typically results when the pH decreases or increases from the optimum pH range. This happens as a result of reversed ionization and deionization of acidic and basic amino acids, which are present at the active site of the enzyme. At higher and lower pH ranges the above ionization and deionization reaction becomes irreversible [92]. This might be a reason for the loss of activity obtained for rHaCat at pH 4 and pH 10 (Fig. 8). The pH study on bovine hydrogen peroxidase with three different pH conditions showed the highest activity at pH 7 and no enzyme activity at pH 1 [93]. The optimum pH of rHaCat was slightly varied from the optimum pH for catalase (pH 7) [88]. Previous studies on catalase from rock bream showed the highest activity at pH 6.5 [30], and disk abalone catalase exhibited over 90% activity at pH 4.5 to 10.5 [31]. According to the observations, rHaCat could withstand the oxidative stress produced by H_2O_2 under a wide range of temperatures and pH conditions.

Clearance of ROS by HaCat was further confirmed through oxidative DNA damage prevention by using varying concentrations of rHaCat. DNA damage prevention was clearly observed using the metal catalyzed MFO assay (Fig. 9). Increasing intensities of supercoiled plasmid bands and reducing band intensities of nicked form plasmids with increasing recombinant protein concentration indicated that the hydroxyl radicals formed by Fenton type reactions were efficiently removed by rHaCat.

Moreover, reaction with rMBP protein and the reaction without protein resulted only an intense band belonging to the nicked form. Moreover, the peroxidase activity of rMBP portion of the fusion protein was insignificant. In previous studies, a faded band was obtained for a nicked plasmid with black rockfish catalase compared to rMBP [29]. These results collectively affirmed that rHaCat effectively removed H_2O_2 from the mixture.

MTT assay determined the cell proliferation rate and cell viability. The metabolically active cells reduced the yellow tetrazolium MTT through dehydrogenase enzyme activity and resulted in intracellular purple formazan formation [94]. The current study confirms the role of HaCat in cell-survival under conditions of oxidative stress. Negligible effects on cell-viability obtained for rMBP pretreated sample (3), confirmed that the ROS removal ability of rHaCat is not derived from the MBP part of the rHaCat fusion protein. Recent studies found suppression of catalase through gene silencing or pharmacological inhibition results in ROS accumulation [95]. It has been documented that the mechanism for H_2O_2 resistance increases with the expression and subsequent activity of catalase in *Lepeophtheirus salmonis* [96]. Catalase activity was suggested as one of the factors involved in determining the cell survival rate in ROS encountered cells [97]. Altogether, the previous evidences and our observations suggest that rHaCat has a potential role in protecting cells during oxidative stress by reducing the oxidative form of H_2O_2 into the non-oxidative form of H_2O.

5. Conclusion

In current study, catalase cDNA from *Hippocampus abdominalis* was identified and molecularly characterized based on its structure and function. The *in-silico* study showed that HaCat consists of a typical domain architecture similar to that of known catalase counterparts. Functional properties of rHaCat were affirmed experimentally by peroxidase activity. The basal level of HaCat mRNA was detected in all examined tissues to a varying degree. Temporal *HaCat* mRNA expression profiles in the blood, liver and kidney demonstrated differential modulation of *HaCat* transcription upon immune stimulation. Collectively, these results contribute to proving the immunological role and antioxidant properties of HaCat in big-belly seahorse.

Acknowledgments

This research was a part of the project titled 'Fish Vaccine Research Center', funded by the Ministry of Oceans and Fisheries, Korea.

References

[1] G. Buonocore, S. Perrone, M.L. Tataranno, Oxygen Toxicity: Chemistry and Biology of Reactive Oxygen Species, (2010), https://doi.org/10.1016/j.siny.2010.04.003.
[2] J. Nordberg, E.S.J.J. Arnér, Reactive oxygen species, antioxidants, and the mammalian thioredoxin system 1 1 This review is based on the licentiate thesis "Thioredoxin reductase—interactions with the redox active compounds 1-chloro-2,4-dinitrobenzene and lipoic acid" by Jonas Nordberg, Free Radic. Biol. Med. 31 (2001) 1287–1312, https://doi.org/10.1016/S0891-5849(01)00724-9.
[3] G. Groeger, C. Quiney, T.G. Cotter, Hydrogen peroxide as a cell-survival signaling molecule, Antioxidants Redox Signal. 11 (2009) 2655–2671, https://doi.org/10.1089/ars.2009.2728.
[4] T. Finkel, Oxidant signals and oxidative stress, Curr. Opin. Cell Biol. 15 (2003) 247–254, https://doi.org/10.1016/S0955-0674(03)00002-4.
[5] F.J. Giordano, Oxygen, oxidative stress, hypoxia, and heart failure, J. Clin. Investig. (2005), https://doi.org/10.1172/JCI200524408.
[6] S. Bhattacharya, Free Radicals in Human Health and Disease, (2015), https://doi.org/10.1007/978-81-322-2035-0.
[7] N. Buchon, N.A. Broderick, B. Lemaitre, Gut homeostasis in a microbial world: insights from Drosophila melanogaster, Nat. Rev. Microbiol. 11 (2013) 615–626, https://doi.org/10.1038/nrmicro3074.
[8] A.J. Kowaltowski, N.C. de Souza-Pinto, R.F. Castilho, A.E. Vercesi, Mitochondria and reactive oxygen species, Free Radic. Biol. Med. 47 (2009) 333–343, https://doi.org/10.1016/j.freeradbiomed.2009.05.004.
[9] R. Mittler, Oxidative stress, antioxidants and stress tolerance, Trends Plant Sci. (2002), https://doi.org/10.1016/S1360-1385(02)02312-9.
[10] D.R. Livingstone, P. Lemaire, A. Matthews, L. Peters, D. Bucke, R.J. Law, Pro-oxidant, antioxidant and 7-ethoxyresorufin O-deethylase (EROD) activity responses in liver of Dab (Limanda limanda) exposed to sediment contaminated with hydrocarbons and other chemicals, Mar. Pollut. Bull. 26 (1993) 602–606, https://doi.org/10.1016/0025-326X(93)90498-9.
[11] I. Fridovich, Superoxide radical and superoxide dismutase, Annu. Rev. Biochem. (1995) 97–112.
[12] D. Scibior, H. Czeczot, Catalase: structure, properties, functions, Postepy Hig. Med. Dosw. (2006), https://doi.org/10.1098/rspb.1998.0388.
[13] H. Bauer, S.M. Kanzok, R. Heiner Schirmer, Thioredoxin-2 but not thioredoxin-1 is a substrate of thioredoxin peroxidase-1 from Drosophila melanogaster. Isolation and characterization of a second thioredoxin in D. Melanogaster and evidence for distinct biological functions of Trx-1 and Trx-2, J. Biol. Chem. 277 (2002) 17457–17463, https://doi.org/10.1074/jbc.M200636200.
[14] A. Kashiwagi, K. Kashiwagi, M. Takase, H. Hanada, M. Nakamura, Comparison of catalase in diploid and haploid Rana rugosa using heat and chemical inactivation techniques, Comp. Biochem. Physiol. B Biochem. Mol. Biol. 118 (1997) 499–503, https://doi.org/10.1016/S0305-0491(97)00216-2.
[15] M.G. Klotz, G.R. Klassen, P.C. Loewen, Phylogenetic relationships among prokaryotic and eukaryotic catalases, Mol. Biol. Evol. 14 (1997) 951–958, https://doi.org/10.1093/oxfordjournals.molbev.a025838.
[16] P. Chelikani, I. Fita, P.C. Loewen, Diversity of Sttructures and Properties Among Catalases, Cmls, 2004.
[17] P. Nicholls, Classical catalase: ancient and modern, Arch. Biochem. Biophys. 525 (2012) 95–101, https://doi.org/10.1016/j.abb.2012.01.015.
[18] D.E. Heck, M. Shakarjian, H.D. Kim, J.D. Laskin, A.M. Vetrano, Mechanisms of oxidant generation by catalase, Ann. N. Y. Acad. Sci. 1203 (2010) 120–125, https://doi.org/10.1111/j.1749-6632.2010.05603.x.
[19] P. Chelikani, I. Fita, P.C. Loewen, Diversity of structures and properties among catalases, Cell. Mol. Life Sci. 61 (2004) 192–208, https://doi.org/10.1007/s00018-003-3206-5.
[20] C.D. Putnam, A.S. Arvai, Y. Bourne, J.A. Tainer, Active and inhibited human catalase structures: ligand and NADPH binding and catalytic mechanism, J. Mol. Biol. 296 (2000) 295–309, https://doi.org/10.1006/jmbi.1999.3458.
[21] G.F. Gaetani, A.M. Ferraris, P. Sanna, H.N. Kirkman, A novel NADPH:(bound) NADP + reductase and NADH:(bound) NADP + transhydrogenase function in bovine liver catalase, Biochem. J. (2005), https://doi.org/10.1042/BJ20041495.
[22] P.A. Walton, M. Pizzitelli, Effects of peroxisomal catalase inhibition on mitochondrial function, Front. Physiol. 3 (2012) 1–10, https://doi.org/10.3389/fphys.2012.00108.
[23] L.A. del Rio, Reactive oxygen species and reactive nitrogen species in peroxisomes. Production, scavenging, and role in cell signaling, Plant Physiol. 141 (2006) 330–335, https://doi.org/10.1104/pp.106.078204.
[24] N. Oshino, B. Chance, H. Sies, T. Bücher, The role of H2O2 generation in perfused rat liver and the reaction of catalase compound I and hydrogen donors, Arch. Biochem. Biophys. 154 (1973) 117–131 https://doi.org/10.1016/0003-9861(73)90040-4.
[25] J.N. Lee, R.K. Dutta, Y. Maharjan, Z. qiang Liu, J.Y. Lim, S.J. Kim, D.H. Cho, H.S. So, S.K. Choe, R. Park, Catalase inhibition induces pexophagy through ROS accumulation, Biochem. Biophys. Res. Commun. 501 (2018) 696–702, https://doi.org/10.1016/j.bbrc.2018.05.050.
[26] R. Radi, J.F. Turrens, L.Y. Chang, K.M. Bush, J.D. Crapo, B.A. Freeman, Detection of catalase in rat heart mitochondria, J. Biol. Chem. 266 (1991) 22028–22034.
[27] C.R. M, Regulation of catalases in arabidopsis, Free Radic. Biol. Med. 23 (1997) 489–496, https://doi.org/10.1016/S0891-5849(97)00109-3.
[28] H. Teramoto, M. Inui, H. Yukawa, OxyR acts as a transcriptional repressor of hydrogen peroxide-inducible antioxidant genes in Corynebacterium glutamicum R, FEBS J. 280 (2013) 3298–3312, https://doi.org/10.1111/febs.12312.
[29] D.A.S. Elvitigala, T.T. Priyathilaka, I. Whang, B.H. Nam, J. Lee, A teleostan homolog of catalase from black rockfish (Sebastes schlegelii): insights into functional roles in host antioxidant defense and expressional responses to septic conditions, Fish Shellfish Immunol. 44 (2015) 321–331, https://doi.org/10.1016/j.fsi.2015.02.020.
[30] D.A.S. Elvitigala, H.K.A. Premachandra, I. Whang, T.T. Priyathilaka, E. Kim, B.S. Lim, H.B. Jung, S.Y. Yeo, H.C. Park, J. Lee, Marine teleost ortholog of catalase from rock bream (Oplegnathus fasciatus): molecular perspectives from genomic organization to enzymatic behavior with respect to its potent antioxidant properties, Fish Shellfish Immunol. 35 (2013) 1086–1096, https://doi.org/10.1016/j.fsi.2013.07.013.
[31] P.M. Ekanayake, M. De Zoysa, H.S. Kang, Q. Wan, Y. Jee, Y.H. Lee, S.J. Kim, J. Lee, Cloning, characterization and tissue expression of disk abalone (Haliotis discus discus) catalase, Fish Shellfish Immunol. 24 (2008) 267–278, https://doi.org/10.1016/j.fsi.2007.11.007.
[32] Y.K. Nam, Y.S. Cho, B.N. Choi, K.H. Kim, S.K. Kim, D.S. Kim, Alteration of antioxidant enzymes at the mRNA level during short-term starvation of rockbream Oplegnathus fasciatus, Fish. Sci. (2005), https://doi.org/10.1111/j.1444-2906.2005.01107.x.
[33] B. Chen, L. Tang, Protective effects of catalase on retinal ischemia/reperfusion injury in rats, Exp. Eye Res. 93 (2011) 599–606, https://doi.org/10.1016/j.exer.2011.07.007.
[34] E.M. Ha, C.T. Oh, J.H. Ryu, Y.S. Bae, S.W. Kang, I. hwan Jang, P.T. Brey, W.J. Lee, An antioxidant system required for host protection against gut infection in Drosophila, Dev. Cell 8 (2005) 125–132, https://doi.org/10.1016/j.devcel.2004.11.007.
[35] H.T. Yang, M.C. Yang, J.J. Sun, F. Guo, J.F. Lan, X.W. Wang, X.F. Zhao, J.X. Wang, Catalase eliminates reactive oxygen species and influences the intestinal microbiota of shrimp, Fish Shellfish Immunol. 47 (2015) 63–73, https://doi.org/10.1016/j.fsi.2015.08.021.

[36] J. Xu, M. xing Lu, D. lin Huang, Y. zhou Du, Molecular cloning, characterization, genomic structure and functional analysis of catalase in Chilo suppressalis, J. Asia Pac. Entomol. 20 (2017) 331–336, https://doi.org/10.1016/j.aspen.2016.08.006.
[37] M.L.F. Ternes, L.C. Gerhardinger, A. Schiavetti, Seahorses in focus: Local ecological knowledge of seahorse-watching operators in a tropical estuary, J. Ethnobiol. Ethnomed. 12 (2016) 1–12, https://doi.org/10.1186/s13002-016-0125-8.
[38] P. Seahorse, F. Centre, Life history and ecology of seahorses : implications for conservation and management, J. Fish Biol. 65 (2004) 1–61, https://doi.org/10.1111/j.1095-8649.2004.00429.x.
[39] F. Centre, Trade in Seahorses and Other Fisheries Centre Research Reports vol. 19, (2011).
[40] A.C.J. Vincent, S.J. Foster, H.J. Koldewey, Conservation and management of seahorses and other Syngnathidae, J. Fish Biol. 78 (2011) 1681–1724, https://doi.org/10.1111/j.1095-8649.2011.03003.x.
[41] S. a Lourie, S.J. Foster, E.W.T. Cooper, A.C.J. Vincent, A Guide to the Identification of Seahorses, (2004) http://www.traffic.org/species-reports/traffic_species_fish29.pdf.
[42] C. Woods, Aquaculture of the big-bellied seahorse Hippocampus abdominalis lesson 1827 (Teleostei: Syngnathidae), Thesis 1827 (2007) 251 http://researcharchive.vuw.ac.nz/handle/10063/288.
[43] P.S. Sang, E.H. Jee, K.G. Dennis, H.K. Ji, H.C.J. Casiano, W.J. Jin, C.P. Se, Identification of scuticociliate Philasterides dicentrarchi from indo-pacific seahorses Hippocampus kuda, Afr. J. Microbiol. Res. (2011), https://doi.org/10.5897/AJMR10.294.
[44] H.J. Koldewey, K.M. Martin-Smith, A global review of seahorse aquaculture, Aquaculture 302 (2010) 131–152, https://doi.org/10.1016/j.aquaculture.2009.11.010.
[45] E. Alcaide, C. Gil-Sanz, E. Sanjuán, D. Esteve, C. Amaro, L. Silveira, Vibrio harveyi causes disease in seahorse, Hippocampus sp, J. Fish Dis. 24 (2001) 311–313, https://doi.org/10.1046/j.1365-2761.2001.00297.x.
[46] H. Koldewey, Syngnathid Husbandry in Public Aquariums, (2005), https://doi.org/10.1109/ICME.2008.4607493.
[47] S. McGinnis, T.L. Madden, BLAST: at the core of a powerful and diverse set of sequence analysis tools, Nucleic Acids Res. 32 (2004) 20–25, https://doi.org/10.1093/nar/gkh435.
[48] M. Oh, N. Umasuthan, D.A.S. Elvitigala, Q. Wan, E. Jo, J. Ko, G.E. Noh, S. Shin, S. Rho, J. Lee, First comparative characterization of three distinct ferritin subunits from a teleost: evidence for immune-responsive mRNA expression and iron depriving activity of seahorse (Hippocampus abdominalis) ferritins, Fish Shellfish Immunol. 49 (2016) 450–460, https://doi.org/10.1016/j.fsi.2015.12.039.
[49] K. Okonechnikov, O. Golosova, M. Fursov, A. Varlamov, Y. Vaskin, I. Efremov, O.G. German Grehov, D. Kandrov, K. Rasputin, M. Syabro, T. Tleukenov, Unipro UGENE: a unified bioinformatics toolkit, Bioinformatics 28 (2012) 1166–1167, https://doi.org/10.1093/bioinformatics/bts091.
[50] C.J.A. Sigrist, E. De Castro, L. Cerutti, B.A. Cuche, N. Hulo, A. Bridge, L. Bougueleret, I. Xenarios, New and continuing developments at PROSITE, Nucleic Acids Res. 41 (2013), https://doi.org/10.1093/nar/gks1067.
[51] P. Publisherlocation, B. Central, L. Publisherimprintname, B. Central, A.A. Articlecitationid, A.A. Articlelastpage, R. Onlinedate, A. Articlegrants, A Simple Modular Architecture Research Tool for the Identification of Signaling Domains, (2000).
[52] E. Gasteiger, C. Hoogland, A. Gattiker, S. Duvaud, M.R. Wilkins, R.D. Appel, A. Bairoch, Protein identification and analysis tools on the ExPASy server, Proteomics Protoc. Handb. (2005) 571–607, https://doi.org/10.1385/1-59259-890-0:571.
[53] P. Rice, L. Longden, A. Bleasby, EMBOSS: the European molecular biology open software suite, Trends Genet. 16 (2000) 276–277, https://doi.org/10.1016/S0168-9525(00)02024-2.
[54] M.A. Larkin, G. Blackshields, N.P. Brown, R. Chenna, P.A. Mcgettigan, H. McWilliam, F. Valentin, I.M. Wallace, A. Wilm, R. Lopez, J.D. Thompson, T.J. Gibson, D.G. Higgins, Clustal W and clustal X version 2.0, Bioinformatics 23 (2007) 2947–2948, https://doi.org/10.1093/bioinformatics/btm404.
[55] S. Kumar, G. Stecher, K. Tamura, MEGA7: molecular evolutionary genetics analysis version 7.0 for bigger datasets, Mol. Biol. Evol. 33 (2016) 1870–1874, https://doi.org/10.1093/molbev/msw054.
[56] Y. Zhang, I-TASSER server for protein 3D structure prediction, BMC Bioinf. 9 (2008) 1–8, https://doi.org/10.1186/1471-2105-9-40.
[57] A. Roy, A. Kucukural, Y. Zhang, I-TASSER: a unified platform for automated protein structure and function prediction, Nat. Protoc. 5 (2010) 725–738, https://doi.org/10.1038/nprot.2010.5.
[58] W.L. DeLano, The PyMOL Molecular Graphics System, Schrödinger LLC, 2002, http://www.pymol.org.doi:1.1038/hr.2014.17 , Version 1.7.4.1.
[59] R. Owczarzy, A.V. Tataurov, Y. Wu, J.A. Manthey, K.A. McQuisten, H.G. Almabrazi, K.F. Pedersen, Y. Lin, J. Garretson, N.O. McEntaggart, C.A. Sailor, R.B. Dawson, A.S. Peek, IDT SciTools: a suite for analysis and design of nucleic acid oligomers, Nucleic Acids Res. 36 (2008) 163–169, https://doi.org/10.1093/nar/gkn198.
[60] K.J. Livak, T.D. Schmittgen, Analysis of relative gene expression data using real-time quantitative PCR and the 2-ΔΔCT method, Methods 25 (2001) 402–408, https://doi.org/10.1006/meth.2001.1262.
[61] Marion M. Bradford, A rapid and sensitive method for the quantitation of microgram quantities of protein utilizing the principle of protein-dye binding, Anal. Biochem. (1976), https://doi.org/10.1016/0003-2697(76)90527-3.
[62] H.E. Müller, Detection of hydrogen peroxide produced by microorganisms on an ABTS peroxidase medium, Zentbl. Bakteriol. Mikrobiol. Hyg. 1 Abt Orig. C 259 (1985) 151–154, https://doi.org/10.1016/S0176-6724(85)80045-6.
[63] S.J. Kwon, K. Kim, I.H. Kim, I.K. Yoon, J.W. Park, Strand breaks in DNA induced by a thiol/Fe(III)/O2mixed-function oxidase system and its protection by a yeast antioxidant protein, Biochem. Biophys. Res. Commun. 192 (1993) 772–777, https://doi.org/10.1006/bbrc.1993.1481.
[64] T.T. Priyathilaka, Y. Kim, H.M.V. Udayantha, S. Lee, H.M.L.P.B. Herath, H.H.C. Lakmal, D.A.S. Elvitigala, N. Umasuthan, G.I. Godahewa, S. Il Kang, H.B. Jeong, S.K. Kim, D.J. Kim, B.S. Lim, Identification and molecular characterization of peroxiredoxin 6 from Japanese eel (Anguilla japonica) revealing its potent antioxidant properties and putative immune relevancy, Fish Shellfish Immunol. 51 (2016) 291–302, https://doi.org/10.1016/j.fsi.2015.12.012.
[65] T. Mosmann, Rapid colorimetric assay for cellular growth and survival: application to proliferation and cytotoxicity assays, J. Immunol. Methods (1983), https://doi.org/10.1016/0022-1759(83)90303-4.
[66] F. Di Domenico, E. Head, D.A. Butterfield, M. Perluigi, Oxidative stress and proteostasis network: culprit and casualty of alzheimer's-like neurodegeneration, Adv. Geriatr. (2014) 1–14, https://doi.org/10.1155/2014/527518 2014.
[67] C.M.L. Press, O. Evensen, The morphology of the immune system in teleost fishes, Fish Shellfish Immunol. (1999), https://doi.org/10.1006/fsim.1998.0181.
[68] C.B.R. Martinez, The kidney ☆, Ref. Modul. Life Sci. (2017) 1–8, https://doi.org/10.1016/B978-0-12-809633-8.03171-X.
[69] T. Tadashi, S. Satimaru, Melano-macrophage centers in the aglomerular kidney of the sea horse (Teleosts): morphologic studies on its formation and possible function, Anat. Rec. 226 (2005) 460–470, https://doi.org/10.1002/ar.1092260408.
[70] C. Agius, The Melano-macrophage centres of fish: a review, Fish Immunol, 1985, pp. 85–105, , https://doi.org/10.1016/B978-0-12-469230-5.50011-8.
[71] Y. Yoshioka, T. Kitao, T. Kishino, A. Yamamuro, S. Maeda, Nitric oxide protects macrophages from hydrogen peroxide-induced apoptosis by inducing the formation of catalase, J. Immunol. 176 (2006) 4675–4681, https://doi.org/10.4049/jimmunol.176.8.4675.
[72] J.H. Kim, J.S. Rhee, J.S. Lee, H.U. Dahms, J. Lee, K.N. Han, J.S. Lee, Effect of cadmium exposure on expression of antioxidant gene transcripts in the river pufferfish, Takifugu obscurus (Tetraodontiformes), Comp. Biochem. Physiol. C Toxicol. Pharmacol. 152 (2010) 473–479, https://doi.org/10.1016/j.cbpc.2010.08.002.
[73] J.H. Kim, S.Y. Wang, I.C. Kim, J.S. Ki, S. Raisuddin, J.S. Lee, K.N. Han, Cloning of a river pufferfish (Takifugu obscurus) metallothionein cDNA and study of its induction profile in cadmium-exposed fish, Chemosphere 71 (2008) 1251–1259, https://doi.org/10.1016/j.chemosphere.2007.11.067.
[74] K. Winzer, C.J.F. Van Noorden, A. Köhler, Glucose-6-phosphate dehydrogenase: the key to sex-related xenobiotic toxicity in hepatocytes of European flounder (Platichthys flesus L.)? Aquat. Toxicol. (2002), https://doi.org/10.1016/S0166-445X(01)00215-6.
[75] P.S. Basha, A.U. Rani, Cadmium-induced antioxidant defense mechanism in freshwater teleost Oreochromis mossambicus (Tilapia), Ecotoxicol. Environ. Saf. 56 (2003) 218–221, https://doi.org/10.1016/S0147-6513(03)00028-9.
[76] H. Yu, W. Deng, D. Zhang, Y. Gao, Z. Yang, X. Shi, J. Sun, J. Zhou, H. Ji, Antioxidant defenses of Onychostoma macrolepis in response to thermal stress: insight from mRNA expression and activity of superoxide dismutase and catalase, Fish Shellfish Immunol. 66 (2017) 50–61, https://doi.org/10.1016/j.fsi.2017.04.027.
[77] L.C.D.G. Svistounov Dmitri, N. Zykova Svetlana, C. Cogger Victoria, Alessandra Warren, Aisling C. McMahon, Robin Fraser, Liver Sinusoidal Endothelial Cells and Regulation of Blood Lipoproteins, Dyslipidemia - From Prev. to Treat. (2002), https://doi.org/10.5772/29169.
[78] E. Nagababu, F.J. Chrest, J.M. Rifkind, Hydrogen-peroxide-induced heme degradation in red blood cells: the protective roles of catalase and glutathione peroxidase, Biochim. Biophys. Acta Gen. Subj. (2003), https://doi.org/10.1016/S0304-4165(02)00537-8.
[79] P. Mitchell, D. Tollervey, mRNA turnover, Curr. Opin. Cell Biol. 13 (2001) 320–325, https://doi.org/10.1016/S0955-0674(00)00214-3.
[80] A.T.Y. Lau, Y. Wang, J.-F. Chiu, Reactive oxygen species: current knowledge and applications in cancer research and therapeutic, J. Cell. Biochem. 104 (2008) 657–667, https://doi.org/10.1002/jcb.21655.
[81] C.N. Paiva, M.T. Bozza, Are reactive oxygen species always detrimental to pathogens? Antioxidants Redox Signal. (2014), https://doi.org/10.1089/ars.2013.5447.
[82] C.N. Jenne, P. Kubes, Immune surveillance by the liver, Nat. Immunol. 14 (2013) 996–1006, https://doi.org/10.1038/ni.2691.
[83] C. Llorente, B. Schnabl, Fast-track clearance of bacteria from the liver, Cell Host Microbe (2016), https://doi.org/10.1016/j.chom.2016.06.012.
[84] S. Brattgjerd, Ø. Evensen, A sequential light microscopic and ultrastructural study on the uptake and handling of *Vibrio salmonicida* in phagocytes of the head kidney in experimentally infected atlantic salmon (*Salmo salar* L.), Vet. Pathol. 33 (1996) 55–65, https://doi.org/10.1177/030098589603300106.
[85] J. Napetschnig, H. Wu, Molecular basis of NF-κB signaling, Annu. Rev. Biophys. (2013), https://doi.org/10.1146/annurev-biophys-083012-130338.
[86] D. Crane, R. Holmes, C. Masters, Proteolytic modification of mouse liver catalase, Biochem. Biophys. Res. Commun. 104 (1982) 1567–1572, https://doi.org/10.1016/0006-291X(82)91430-9.
[87] Y. Sun, Multiplicity of antioxidant enzyme catalase in mouse liver cells, Free Radic. Res. 26 (1997) 343–350, https://doi.org/10.3109/10715769709097814.
[88] W.B. Corporation, Introduction to Enzymes, Eff. PH (2015), p. 1, https://doi.org/10.1201/9781420094343-c1.
[89] T. Amo, H. Atomi, T. Imanaka, Unique presence of a manganese catalase in a hyperthermophilic archaeon, Pyrobaculum calidifontis VA1, J. Bacteriol. 184 (2002) 3305–3312, https://doi.org/10.1128/JB.184.12.3305-3312.2002.
[90] M.D.N. Tharuka, S.D.N.K. Bathige, J. Lee, Molecular cloning, biochemical characterization, and expression analysis of two glutathione S-transferase paralogs from the big-belly seahorse (Hippocampus abdominalis), Comp. Biochem. Physiol. B Biochem. Mol. Biol. 214 (2017) 1–11, https://doi.org/10.1016/j.cbpb.2017.08.

005.
[91] J. Ko, Q. Wan, S.D.N.K. Bathige, J. Lee, Molecular characterization, transcriptional profiling, and antibacterial potential of G-type lysozyme from seahorse (Hippocampus abdominalis), Fish Shellfish Immunol. 58 (2016) 622–630, https://doi.org/10.1016/j.fsi.2016.10.014.
[92] W.T. Frankenberger, J.B. Johanson, Effect of pH on enzyme stability in soils, Soil Biol. Biochem. 14 (1982) 433–437, https://doi.org/10.1016/0038-0717(82)90101-8.
[93] J. Eed, Factors affecting enzyme activity, Essaim 10 (2012) 48–51 http://dc.cod.edu/essai%5Cnhttp://dc.cod.edu/essai/vol10/iss1/19%5Cnhttp://alevelnotes.com/Factors-affecting-Enzyme-Activity/146?tree=.
[94] M. Ferrari, M.C. Fornasiero, A.M. Isetta, MTT colorimetric assay for testing macrophage cytotoxic activity in vitro, J. Immunol. Methods 131 (1990) 165–172, https://doi.org/10.1016/0022-1759(90)90187-Z.
[95] J.N. Lee, R.K. Dutta, Y. Maharjan, Z. qiang Liu, J.Y. Lim, S.J. Kim, D.H. Cho, H.S. So, S.K. Choe, R. Park, Catalase inhibition induces pexophagy through ROS accumulation, Biochem. Biophys. Res. Commun. (2018), https://doi.org/10.1016/j.bbrc.2018.05.050.
[96] K.O. Helgesen, M.J. Bakke, K. Kaur, T.E. Horsberg, Increased Catalase Activity — A Possible Resistance Mechanism in Hydrogen Peroxide Resistant Salmon Lice (Lepeophtheirus salmonis), Aquaculture (2017), https://doi.org/10.1016/j.aquaculture.2016.10.012.
[97] L.C. Lin, G.H. Lin, Z.L. Wang, Y.H. Tseng, M.S. Yu, Differential expression of catalases in Vibrio parahaemolyticus under various stress conditions, Res. Microbiol. 166 (2015) 601–608, https://doi.org/10.1016/j.resmic.2015.07.001.